JOURNAL OF Materials CHEMISTRY

Synthesizing nanocrystalline $LiMn_2O_4$ by a combustion route

Daniela Kovacheva,[a] Hristo Gadjov,[a] Kostadin Petrov,[a] Sankar Mandal,[b] Mónica. G. Lazarraga,[b] Laura Pascual,[b] J. Manuel Amarilla,[b] Rosa M. Rojas,[b] Pilar Herrero[b] and José M. Rojo*[b]

[a]*Institute of General and Inorganic Chemistry, Bulgarian Academy of Science, 1113 Sofia, Bulgaria*
[b]*Instituto de Ciencia de Materiales de Madrid, Consejo Superior de Investigaciones Científicas, Cantoblanco, 28049 Madrid, Spain. E-mail: jmrojo@icmm.csic.es*

Received 23rd August 2001, Accepted 25th January 2002
First published as an Advance Article on the web 5th March 2002

Nanocrystalline samples of lithium manganese oxide with cubic spinel structure have been prepared by combustion of reaction mixtures containing Li(I) and Mn(II) nitrates that operate as oxidisers, and sucrose that acts as fuel. The samples were characterised by X-ray diffraction, transmission electron microscopy, thermal analysis, and impedance and electrochemical measurements. The effect of the fuel content on the purity and morphology of the products was analysed. The samples as prepared showed small amounts of Mn_2O_3 and Mn_3O_4 as impurities, depending on the amount of sucrose used in the synthesis. Annealing at 700 °C led to single-phase cubic spinels. In these phases, the smallest average particle size (*ca.* 30 nm) corresponded to the sample obtained with a hyperstoichiometric amount of fuel. This sample showed the $Li_{1.05}Mn_{1.95}O_4$ composition as deduced from the thermal and electrochemical data. No variation in conductivity associated with the cubic⇔orthorhombic phase transition was observed. The electrochemical behaviour as positive electrode showed good cyclability at high current densities (reversible capacity of 73 mAh g^{-1} at 2.46 mA cm^{-2}).

Introduction

$LiMn_2O_4$ is a promising positive electrode material for rechargeable lithium-ion batteries because of its high reduction potential (4 V), low cost, and acceptable environmental impact.[1–4] Attempts at improving the electrochemical response have been addressed in two ways: (i) by appropriate processing of composites having $LiMn_2O_4$ as active material, and (ii) by modifying the active material in order to overcome the loss of capacity on cycling. Regarding the first point, the capacity can change from 0 to 135 mAh g^{-1} as a function of the carbon black content according to a percolation process.[5] Regarding the second aspect, samples with a chemical composition slightly different from stoichiometric $LiMn_2O_4$ and/or samples of the nominal $LiMn_2O_4$ composition have been prepared by different synthesis procedures.

$LiMn_{2-x}M_xO_4$ compounds in which Mn is partially substituted by either iso- or alio-valent cations such as M = Co, Fe, Al, Cr, Ni, or even Li have been obtained. These compounds show better cycling performance at *ca.* 4 V compared to $LiMn_2O_4$.[6–12] The nominal $LiMn_2O_4$ compound has been obtained at moderate temperature by different methods, such as sol–gel, Pechini, and microwave.[13–15] The sol–gel method yields powder samples with small particle size but with some impurities of manganese oxides. To remove the impurities and to get pure materials, the powder samples are usually calcined up to 800 °C but it causes a net increase in the particle size.[13] The Pechini method affords materials that show high cyclability but low capacity.[14] The microwave method leads to samples in which the particle shape and size seem to depend on the starting manganese oxide used as the reagent.[15] Moreover, the capacity also depends on the firing temperature; thus, a maximum capacity for firing temperatures in the range 700–750 °C has been reported.[16]

Another synthesis procedure that yields finely divided powders is the so-called combustion route. It is based on the reaction between inorganic reagents (generally nitrates) and organic fuels (tetraformal triazine TFTA, urea, citric acid, *etc.*).[17–21] The intense evolution of the gases during the reaction causes the formation of a voluminous product consisting of loosely packed particles. In this paper we describe the synthesis of nanocrystalline $LiMn_2O_4$ by a combustion method, in which lithium(I) and manganese(II) nitrates are the reagents, and sucrose (commercial sugar) is the fuel. The effect of the sugar content on the purity and morphology of the samples is analysed. The samples are characterised by X-ray diffraction, thermal analysis, and impedance spectroscopy. The electrochemical response of the samples as active materials for cathodes is also studied, and the capacity and cyclability are discussed in relation to the particle size.

Experimental

Samples were prepared by slow evaporation and ignition of a reaction mixture containing Li(I) nitrate, Mn(II) nitrate and sucrose according to the formal chemical equation:

$$24\,LiNO_3 + 48\,Mn(NO_3)_2 + 11\,C_{12}H_{22}O_{11} \rightarrow 24\,LiMn_2O_4 + 60\,N_2 + 132\,CO_2 + 121\,H_2O \quad (1)$$

The amounts of the reagents were calculated to obtain 3 g of $LiMn_2O_4$. As starting compounds, Li_2CO_3, $Mn(NO_3)_2{\cdot}4H_2O$ and sucrose, all of reagent-grade purity, were used. The stoichiometric mixture of Li_2CO_3 and $Mn(NO_3)_2{\cdot}4H_2O$ was placed in a Pyrex glass dish of *ca.* 400 cm^3 and dissolved in a minimum quantity of dilute HNO_3. The preset amount of sucrose dissolved in 20 ml of water was added to the solution. The dish containing the reaction mixture was placed on an electric heater and kept at 120 °C. At this temperature the liquid evaporated, and the residual viscous mass transformed into brownish-yellow foam. When ignited, it burned without flame yielding a voluminous, black, sponge-like substance.

The stoichiometric mixture of the nitrates and sucrose was

 DOI: 10.1039/b107669h

calculated on the basis of the total oxidising and reducing valence of the metal nitrates (O) and the sucrose (F) according to F : O = 1.[22,23] Eqn. (1) fulfills this condition.

Experiments were also carried out with half-stoichiometric (F : O = 0.5), and double-stoichiometric (F : O = 2) amounts of the sucrose. The samples thus prepared are referred to hereafter as 0.5P, 1P, 2P, where the coefficient denotes the F : O ratio and P stands for as prepared. A part of these samples was annealed at 700 °C for 1 h in still air. The samples thus treated are referred as 0.5A, 1A, and 2A, where A stands for annealed.

Chemical analyses were made by the IPC-MS technique. The 2A sample was dissolved in HCl and H_2O_2, and the Li and Mn contents were determined.

X-Ray powder diffraction (XRD) patterns were recorded at room temperature with a Siemens D501 diffractometer, with CuKα radiation. The patterns were recorded in the step-scanning mode at 0.02°(2θ) and 1 s step^{-1} counting time within the range $10° \leqslant 2\theta \leqslant 80°$. Lattice parameters were refined with the CelRef program.[24]

Transmission electron (TEM) micrographs were taken in a JEOL 2000 FX microscope operating at an acceleration voltage of 200 kV and equipped with a $\pm 45°$ double-tilt sample holder. The samples were dispersed in acetone; drops of the dispersion were transferred to a holey carbon-coated copper grid.

Thermogravimetric (TG) analyses were made on a Stanton STA781 instrument in still air atmosphere up to 1200 °C, at a 2 °C min^{-1} heating/cooling rate. A sample of *ca.* 15 mg was used in each run. Differential scanning calorimetry (DSC) curves were obtained in a Seiko 320U instrument, between −60 and 60 °C in still air atmosphere, and a 10 °C min^{-1} heating/cooling rate.

Two-probe impedance measurements were carried out in a 1260 Solartron impedance/gain phase analyser. The frequency range used was 5–10^6 Hz. Cylindrical pellets were prepared by cold pressing, and sintering at 700 °C for 3 h. This thermal treatment is similar to that chosen for preparing the annealed samples. Silver electrodes were used. The pellets were mounted in an Oxford cryostat. The electrical measurements were done at state temperatures (from –150 to 80 °C) with the pellets in still, dry nitrogen.

The electrochemical behaviour was analysed in a lithium cell. Positive electrode composites were prepared from spinel powder ($\approx$20 mg or 72 wt.%), MMM Super P carbon black (17 wt.%) and poly(vinylidene fluoride) (PVDF, 11 wt.%). PVDF was dissolved in *N*-methylpyrrolidone, and the other two components were added to the solution. The solvent was evaporated at 110 °C, and cylindrical pellets (13 mm diameter) of the composites were obtained by cold pressing. The electrolyte used was a 1 M solution of $LiPF_6$ in ethylene carbonate and dimethyl carbonate as supplied by Merck. The negative electrode was a lithium foil, which also operated as reference electrode. The components were assembled into a two-electrode Swagelock cell within an argon glove box in which water content was kept below 1 ppm. The cells thus fabricated were cycled galvanostatically at room temperature in the voltage range of 3–5 V. The current densities chosen in the discharge stage were 0.20, 0.49 and 2.46 mA cm^{-2}, which correspond to C/12, C/5 and C. C is the capacity of the electrode calculated on the basis of the theoretical capacity of $LiMn_2O_4$, which is equal to 148 mAh g^{-1}. The experiments were made in an Arbin battery tester system (BT2043).

Results and discussion

Structural and morphological characterisation

The X-ray diffraction patterns of the as prepared (P) and annealed (A) samples are shown in Fig. 1. The patterns of the P samples show broad diffraction lines of the spinel phase along with weaker lines of an impurity of Mn_2O_3 [sample 0.5P, Fig. 1(a)] or Mn_3O_4 [samples 1P and 2P, Fig. 1(b),(c)]. In air atmosphere manganese nitrate decomposes into MnO_2 that transforms into Mn_2O_3 at about 600 °C, and Mn_2O_3 transforms into Mn_3O_4 at about 900 °C.[25] Taking this into account the presence of Mn_2O_3 in the 0.5P sample and of Mn_3O_4 in the 1P and 2P samples indicates that the reaction temperature is lower for low sucrose content (F : O $<$1) and higher for high sucrose content (F : O $\geqslant$1). The amount of Mn_3O_4 in the 2P sample was *ca.* 11% by volume as estimated from the PowderCell programme.[26]

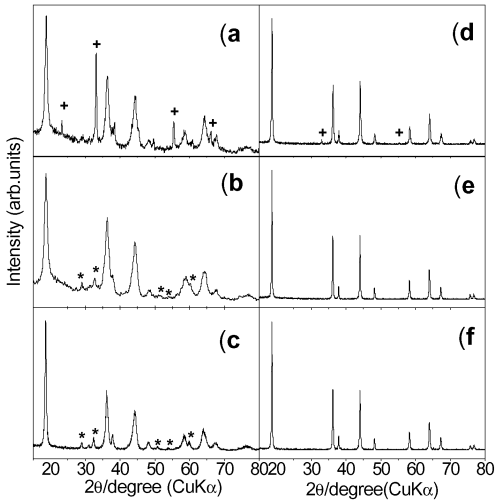

Fig. 1 X-Ray powder diffraction patterns recorded for the samples: 0.5P (a), 1P (b), 2P (c), 0.5A (d), 1A (e), and 2A (f). Crosses and stars stand for Mn_2O_3 and Mn_3O_4, respectively.

The X-ray diffraction patterns recorded for the annealed 1A and 2A samples [Fig. 1(e),(f)] only show the typical peaks of the spinel structure. The pattern of the 0.5A sample [Fig. 1(d)] shows, besides the peaks of the spinel structure, some peaks of Mn_2O_3; however, these are rather less intense than the peaks observed in the corresponding 0.5P sample [Fig.1(a)]. This result, together with the lack of impurity in the 1A and 2A samples, indicates that the annealing treatment leads to single phases. The 0.5A sample was excluded from further measurements. The cubic lattice parameters determined for the pure 1A and 2A sample are 8.236(2) and 8.233(1) Å, respectively. These values are very close each other but they are smaller than the lattice parameter reported for the stoichiometric $LiMn_2O_4$, a = 8.248(2) Å.[27,28] Since small lattice parameters are associated with hyperstoichiometry of lithium such as $Li_{1+x}Mn_{2-x}O_4$ ($0 \leqslant x \leqslant 0.24$),[3,28,29] the lattice parameters found seem to indicate that we are dealing with lithium excess samples.

The TEM image recorded for the 2A sample is shown as an example in Fig. 2. It consists of aggregated particles of about 30 nm in size. A more detailed analysis of the particle size for the 1A and 2A samples is shown in the histograms of Fig. 3. In the two cases a maximum in particle size is observed. When the histograms of the 1A and 2A samples are compared we observe that in the former sample the size distribution is broader and the maximum is shifted towards higher size. Indeed, the average particle size and the standard deviation are 55 and 23 nm, respectively, for the 1A sample, and 33 and 12 nm, respectively, for the 2A sample. It indicates that when the samples are prepared by using a high sucrose content, the particles are slightly smaller and the distribution is more homogeneous. Both effects are associated with the large amount of gases evolved during the combustion reaction for the high sucrose content; the gases hinder coalescence and subsequent growth of the particles.

From the X-ray diffraction and TEM results it is clear that nanocrystalline particles of the spinel phase can be obtained by the combustion method developed. A high sucrose content

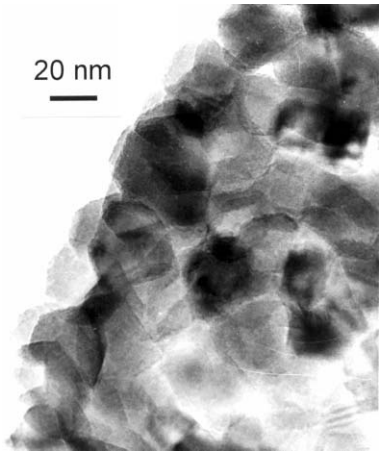

Fig. 2 Transmission electron micrograph obtained for the 2A sample.

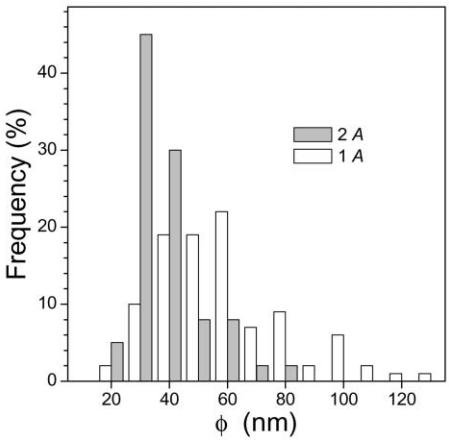

Fig. 3 Size distribution histogram of the samples: 1A (white bar), and 2A (light grey bar).

leads to samples with low particle size, but a subsequent annealing at 700 °C is needed to get pure samples. According to our results the 2A sample is the most outstanding one, and hence we have studied the electrical and electrochemical properties of that sample.

Electrical and electrochemical characterisation

Stoichiometric $LiMn_2O_4$ is an n-type semiconductor in which the dc conductivity increases by approximately one order of magnitude as the low-temperature phase (orthorhombic) is transformed into the high-temperature phase (cubic) at temperatures close to room temperature.[30–33] The dc conductivity of a pellet of the 2A sample was very close to the grain interior dc conductivity as deduced from an analysis of the conductivity *vs.* frequency (not shown). The dc conductivity (σT) *vs.* reciprocal temperature ($1000/T$) is plotted in Fig. 4(a). At temperatures above 180 K ($1000/T < 5.5$) a linear dependence is observed. Such behaviour agrees with the Mott model of phonon-assisted hopping of small polaron among transition metal ions in two-valence states,[34] *i.e.* electron hopping through nearest neighbours, Mn^{3+}/Mn^{4+} in our case. The experimental data are well fitted to the expression:

$$\sigma T = v_0[e^2c(1 - c)/k_BR]\exp(-2\alpha R)\exp(-W/k_BT) \quad (2)$$

where v_0 is the optical phonon frequency (1.8×10^{-13} s^{-1} as deduced from the IR spectrum),[35] e is the charge of the electron, c is the $Mn^{3+}/(Mn^{3+}+Mn^{4+})$ ratio (*ca.* 0.5 in our case), k_B is the Boltzmann constant, T is the temperature, R is the Mn–Mn distance (2.91 Å as deduced from $R = a\sqrt{2}/4$, where a is the cubic lattice parameter), α^{-1} is the localisation length of the s-like wave function which describes the localised state at each transition metal site, and W is the activation energy for hopping. A W value of 0.37 eV was deduced from the fitting; this value is close to the values reported for the cubic phase of the $LiMn_2O_4$ spinel.[13,32,33]

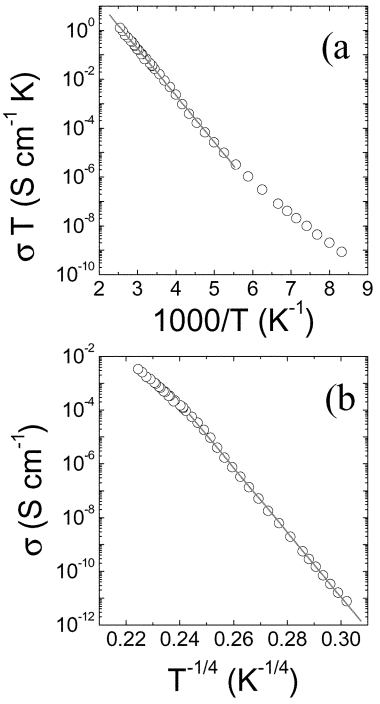

Fig. 4 Temperature dependence of dc conductivity for the 2A sample: a) σT *vs.* $1000/T$; b) σ *vs.* $T^{-1/4}$. From the fittings (solid lines) we have deduced $W = 0.37$ eV, $\alpha = 0.27$ Å^{-1}, $N(E_F) = 8.8 \times 10^{17}$ eV^{-1} cm^{-3}.

At low temperatures (below 180 K), the experimental data of Fig. 4(a) depart systematically out from the straight line and cannot be fitted to eqn. (2). However, the temperature dependence of conductivity can be described by the variable-range-hopping model.[36] According to this model, electron hopping occurs preferentially beyond the nearest neighbour Mn ions at different energies, these energies being lower than the energy required for hopping among nearest neighbour Mn ions (0.37 eV). The temperature dependence of the dc conductivity follows the expression:

$$\sigma = \sigma_0\exp[(-T_0/T)]^{1/4} \quad (3)$$

where σ_0 is a constant and $T_0 = 19.44\alpha^3/k_BN(E_F)$; $N(E_F)$ is the density of states at the Fermi level. The linear dependence observed in the plot of σ *vs.* $T^{-1/4}$ [Fig. 4(b)] indicates that the variable-range-hopping model accounts for the dc conductivity at low temperatures.

It is worth noting that the dc conductivity does not show any sharp variation at temperatures close to room temperature, the variation being associated with the well-known cubic ($Fd3m$)⇔ orthorhombic ($Fddd$) phase transition for $LiMn_2O_4$. The lack in the DSC curve of any exo-/endo-thermic peak confirms that the 2A sample does not undergo any phase transition. This result is contrary to that reported for stoichiometric $LiMn_2O_4$ and points to a lithium content higher than one Li^+ per formula in our 2A sample.[31,37] Gao and Dahn have developed a procedure that allows the estimation of the lithium content x in $Li_{1+x}Mn_{2-x}O_4$ from TG data, *i.e.* from the plot of the temperature at the onset of the weight loss, the so-called T_{c1}, *vs.* x.[38,39] To estimate the lithium content of the 2A sample, its TG curve was recorded (Fig. 5) and we measured $T_{c1} = 780$ °C. From this value and the plot of T_{c1} *vs.* x already

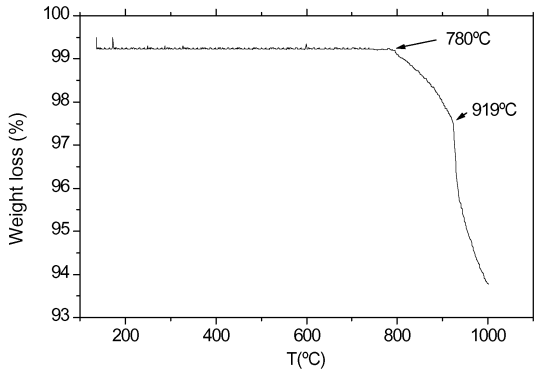

Fig. 5 TG curve recorded for the 2A sample at 2 °C min^{-1} in still air.

mentioned,[38] $x = 0.05$ was deduced. Thus, the formula for the 2A sample is $Li_{1.05}Mn_{1.95}O_4$, which can be expressed as $(Li)_{8a}[Li_{0.05}Mn^{3+}{}_{0.85}Mn^{4+}{}_{1.1}]_{16d}O_4$ where the subscripts 8a and 16d stand for the tetrahedral and octahedral sites, respectively, in the cubic spinel. From chemical analysis we found a Li and Mn content of 4.02 and 60.2 wt%, respectively. These values agree with those deduced for Li (4.08 wt%) and Mn (60.0 wt%) from the $Li_{1.05}Mn_{1.95}O_4$ formula. The value $x = 0.05$ also agrees with the value $x = 0.06$ deduced from the plot of the cubic lattice parameter *vs.* x.[38]

The charge and discharge curves at several cycles obtained under three current densities are shown in Fig. 6. Besides the two main plateaux around 4 V, we observe short plateaux at *ca.* 4.3 V in charge and at *ca.* 3.3 V in discharge for the curves recorded at low current density (0.20 mA cm^{-2}). These short plateaux have also been found in slightly non-stoichiometric $LiMn_2O_4$ samples.[39,40]

In Fig. 7 we have plotted the discharge capacity *vs.* cycle number for the three current densities. The discharge capacity of the first cycle recorded at 0.20 mA cm^{-2} is as high as 131 mAh g^{-1}. It corresponds to 0.88 Li^+ inserted, and indicates that the pristine spinel has 0.88 Mn^{3+}. From this value we have estimated a $Li_{1.04}Mn_{1.96}O_4$ composition, which agrees fairly with the composition determined from the T_{c1} and the chemical analysis. In Fig. 7 we also observe a continuous decrease in capacity as the current density increases from 0.20 to 0.49 mA cm^{-2}. However, we observe a sharp decrease in capacity as the current density changes from 0.49 to 2.46 mA cm^{-2}; at the latter value the reversible capacity is 73 mAh g^{-1}. At low currents the kinetic limitations do not rule, and the insertion/extraction of Li^+ ions into/from the bulk of the particles is favoured. In accordance with it, the capacity is high. At high

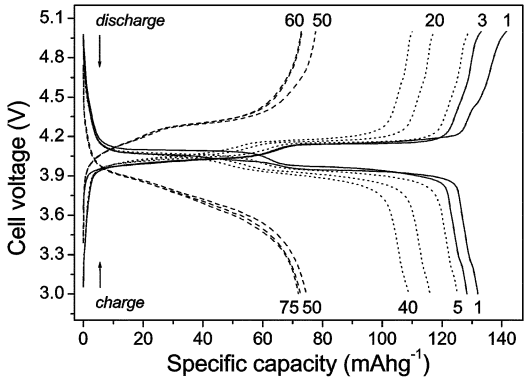

Fig. 6 Charge and discharge curves of the indicated cycles recorded at several current densities (*j*). Solid lines stand for $j = 0.20$ mA cm^{-2} (C/12) both in charge and discharge. Dotted lines stand for $j = 0.31$ mA cm^{-2} (C/8) in charge and $j = 0.49$ mA cm^{-2} (C/5) in discharge. Dashed lines stand for $j = 1.23$ mA cm^{-2} (C/2) in charge and $j = 2.46$ mA cm^{-2} (C) in discharge.

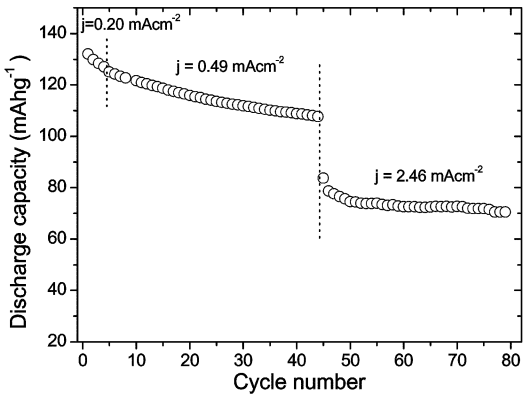

Fig. 7 Discharge capacity *vs.* cycle number for the 2A sample at the current densities indicated.

currents, only the outer part of the particles undergoes the insertion/extraction of Li^+ ions, and hence the capacity is low. We have compared the capacity of the 2A sample with that of a $LiMn_2O_4$ sample we prepared by solid-state reaction, and whose particle size was of the order of 1 μm. The reversible capacity of the latter sample at high current density (2.46 mA cm^{-2}) is 60 mAh g^{-1}, *i.e.* 17% lower than the capacity of the 2A sample. The higher capacity found for the 2A sample can be explained by the smaller particle size of this sample.

A slow fade of capacity on cycling is observed in Fig. 7. Assuming a linear decrease of the capacity, the capacity lost per cycle is 1.2% at 0.20 mA cm^{-2}, 0.32% at 0.49 mA cm^{-2}, and 0.08% at 2.46 mA cm^{-2}. It is worth noting that the rates are very low, even lower than that reported for stoichiometric $LiMn_2O_4$.[21] The good cyclability shown by the 2A sample can be associated with the slight excess of lithium present in this sample. Moreover, the gradual decrease in the rate of capacity fade on increasing the current density shows that the reversibility is enhanced at high current density, *i.e.* the insertion/extraction of the Li^+ ions is more reversible when it occurs preferentially in the outer part of the particles.

Concluding remarks

Samples having a slight excess of lithium (1.05 Li per formula) and cubic spinel-type structure were prepared by a combustion method in which a new and very low-cost material, sugar, was used as fuel. The self-combustion process that propagates in a foamy reaction body is time-saving, and allows preparation of practically pure nanocrystalline products. Annealing at 700 °C yields single phases with a particle size of *ca.* 30 nm. These samples show a good cyclability at high current density when they are used as positive electrodes in a lithium cell.

Acknowledgements

The support by the Spanish CSIC and the Bulgarian Academy of Science through a joint research project (2001BG0002) is gratefully acknowledged. The Spanish authors also thank the CICYT and CAM for financial support through the projects MAT 98-0904 and 07N/0059/1998, respectively. S. M. and M.G. L. thank to the Spanish Education and Culture Ministry for their respective fellowships.

References

1 M. M. Thackeray, W. I. F. David, P. G. Bruce and J. B. Goodenough, *Mater. Res. Bull.*, 1983, **18**, 461.
2 J. M. Tarascon, E. Wang, F. Shokoohi, W. R. McKinnon and S. Colson, *J. Electrochem. Soc.*, 1991, **137**, 2864.
3 R. J. Gummow, A. de Kock and M. M. Thackeray, *Solid State Ionics*, 1994, **69**, 59.

4 M. M. Thackeray, *Prog. Solid State Chem.*, 1997, **25**, 1.
5 S. Mandal, J. M. Amarilla, J. Ibañez and J. M. Rojo, *J. Electrochem. Soc.*, 2001, **148**, 24.
6 l. Guohua, H. Ikuta, T. Uchida and M. Wakihara, *J. Electrochem. Soc.*, 1996, **143**, 178.
7 M. Hosoya, H. Okuta and M. Wakihara, *Solid State Ionics*, 1998, **111**, 153.
8 H. Kawai, M. Nagata, H. Kageyama, H. Tukamoto and A. R. West, *Electrochim. Acta*, 1999, **45**, 315.
9 T. Ohzuku, K. Ariyosi, S. Takeda and Y. Sakai, *Electrochim. Acta*, 2001, **46**, 2327.
10 C. Sigala, A. Verbaere, J. L. Mansot, D. Guyomard, Y. Piffard and M. Tournoux, *J. Solid State Chem.*, 1997, **132**, 372.
11 Y. Xia, T. Sakai, T. Fujieda, M. Wada and H. Yoshinaga, *Electrochem. Solid-State Lett.*, 2001, **4**, 9.
12 Y. Ein-Eli and W. F. Howard, Jr, *J. Electrochem. Soc.*, 1997, **144**, L205.
13 V. Massaroti, D. Capsoni, M. Bini, G. Chiodelli, C. B. Azzoni, M. C. Mozzati and A. Paleari, *J. Solid State Chem.*, 1999, **147**, 509.
14 W. Liu, G. C. Farrington, F. Chaput and B. Dunn, *J. Electrochem. Soc.*, 1996, **143**, 879.
15 H. Yang, X. Huang and L. Chen, *J. Power Sources*, 1999, **81–82**, 647.
16 V. Manev, B. Banov, A. Momchilov and A. Nassalevska, *J. Power Sources*, 1995, **57**, 99.
17 S. S. Manoharan, N. R. S. Kumar and K. C. Patil, *Mater. Res. Bull.*, 1990, **25**, 731.
18 S. Bhaduri, S. B. Bhaduri and K. A. Prisbrey, *J. Mater. Res.*, 2000, **14**, 3571.
19 W. Yang, G. Zhang, J. Xie, L. Yang and Q. Liu, *J. Power Sources*, 1999, **81–82**, 412.
20 S. Chitra, P. Kalyani, T. Mohan, R. Gangadharan, B. Yebka, S. Castro-Gracia, M. Massot, C. Julien and M. Eddrief, *J. Electroceram.*, 1999, **3**, 433.
21 W. Yang, Q. Liu, W. Qiu, S. Lu and L. Yang, *Solid State Ionics*, 1999, **121**, 79.
22 S. R. Jain, K. C. Adiga and V. R. Pai Verneker, *Combust. Flame*, 1981, **40**, 71.
23 M. M. A. Sekar and K. C. Patil, *J. Mater. Chem.*, 1992, **2**, 739.
24 J. Laugier and A. Filhol, CelRef, PC version (unpublished), ILL, Grenoble, France, 1991.
25 R. C. Mackenzie, in *Differential Thermal Analysis*, R. C. Mackenzie, ed., Academic Press, London. 1970, vol. 1, ch. 9 and 13.
26 W. Kraus and G. Nolze, PowderCell program for Windows, Version 2.3, BAM, Berlin, 1999.
27 G. Rousse, C. Masquelier, J. Rodríguez-Carvajal and M. Hervieu, *Electrochem. Solid State Lett.*, 1999, **2**, 6.
28 J. M. Paulsen and J. R. Dahn, *Chem. Mater.*, 1999, **11**, 3065.
29 G. G. Amatucci, C. N. Schmutz, A. Blyr, C. Sigala, A. S. Gozdz, D. Larcher and J. M. Tarascon, *J. Power Sources*, 1997, **69**, 11.
30 J. B. Goodenough, A. Manthiran and P. Wnetrzewski, *J. Power Sources*, 1993, **43**, 269.
31 Y. Shimakawa, T. Numata and J. Tabuchi, *J. Solid State Chem.*, 1997, **131**, 138.
32 J. Sugiyama, T. Atsumi, A. Koiwai, T. Sasaki, T. Hioki, S. Noda and N. Kamegashira, *J. Phys.: Condens. Matter*, 1997, **9**, 1729.
33 J. Molenda, K. Swierczek, W. Kucza, J. Marzec and A. Stoklosa , *Solid State Ionics*, 1999, **123**, 155.
34 N. F. Mott, *J. Non-Cryst. Solids*, 1968, **1**, 1.
35 R. K. Stoyanova, E. N. Zhecheva and M. Gorova, *J. Mater. Chem.*, 2000, **10**, 1377.
36 N. F. Mott, *Philos. Mag.*, 1969, **19**, 835.
37 A. Yamada, *J. Solid State Chem.*, 1996, **122**, 160.
38 Y. Gao and J. R. Dahn, *Appl. Phys. Lett.*, 1995, **66**, 2487.
39 Y. Gao and J. R. Dahn, *J. Electrochem. Soc.*, 1996, **143**, 100.
40 M. R. Palacin, Y. Chabre, L. Dupont, M. Hervieu, P. Strobel, G. Rousse, C. Masquelier, M. Anne, G. G. Amatucci and J. M. Tarascon, *J. Electrochem. Soc.*, 2000, **147**, 848.